Finite temperature many-body effects in half-metallic ferromagnets

Andreas Weh, Junya Otsuki, Liviu Chioncel

Angaben zur Veröffentlichung / Publication details:

Weh, Andreas, Junya Otsuki, and Liviu Chioncel. 2020. "Finite temperature many-body effects in half-metallic ferromagnets." *JPS Conference Proceedings* 30: 011005. https://doi.org/10.7566/jpscp.30.011005.

Proc. Int. Conf. Strongly Correlated Electron Systems (SCES2019)
JPS Conf. Proc. **30**, 011005 (2020)
https://doi.org/10.7566/JPSCP.30.011005

Finite Temperature Many-body Effects in Half-metallic Ferromagnets

Andreas Weh[1], Junya Otsuki[2], Liviu Chioncel[3,4]

Theoretical Physics II, Institute of Physics, University of Augsburg, 86135 Augsburg, Germany
Research Institute for Interdisciplinary Science, Okayama University, Okayama 700–8530, Japan
Augsburg Center for Innovative Technologies, University of Augsburg, 86135 Augsburg, Germany
Theoretical Physics III, Center for Electronic Correlations and Magnetism, Institute of Physics, University of Augsburg, 86135 Augsburg, German

E-mail: andreas.weh@physik.uni-augsburg.de

(Received September 16, 2019)

The signature of electronic correlations in the band structure of half-metallic ferromagnets is the appearance of nonquasiparticle states (NQP) in the vicinity of the Fermi level. Here we discuss the finite temperature behavior of the NQP solving the fully polarized Hubbard model in infinite dimensions using the continuous-time quantum Monte Carlo solver of the dynamical mean field theory. We discuss the existence of various features of the spectral functions of half-metallic ferromagnets and show numerically that for the bulk system the tail of the NQP states vanishes exactly at the Fermi level at low temperatures.

KEYWORDS: half-metallic ferromagnet, nonquasiparticle states, DMFT, CT-QMC, analytic continuation

1. Introduction

Half-metals are magnetic materials that exhibit a metallic spectral function at the Fermi level for one spin channel and simultaneously a band gap for the other spin channel. These half-metallic magnetic materials show great promise for spintronic devices [1,2]. Half-metallic electrodes could provide fully spin-polarized currents and large magnetoresistance in giant-magnetoresistance and tunnel-magnetoresistance devices [2]. Density Functional Theory (DFT) studies have identified a number of half-metallic bulk compounds, including Heusler alloys [3], double perovskites, transition metal oxides, chalcogenides and pnictides. Some of these proposed materials have been realized in experiments. Within the DFT, modeling of the ground state properties of these materials from a single particle picture became accessible. However, the physics in correlated electron systems is essentially many-body and concepts such as band theory are expected to fail [4,5]. In particular, in metallic ferromagnets spin fluctuations play a crucial role [6]. Therefore, in these materials the scattering of charge carriers on such magnetic excitations is expected to influence the macroscopic properties including transport. In itinerant ferromagnets states near the Fermi level are quasiparticles for both spin projections; in half-metallic ferromagnets (HMFs), however, incoherent nonquasiparticle (NQP) states play an important role. These NQP states occur near the Fermi level in the energy gap [7–9]. The density of the NQP states vanishes at the Fermi level but increases at an energy scale of the order of the characteristic magnon-frequency. The NQP contribution to the density of states

and transport properties have been calculated also from the first principles DFT+DMFT theory for some materials such as the prototype HMF, NiMnSb [10], or other Heusler alloys [11], zincblende structure compounds [12, 13] and CrO_2 [14].

2. Computational Method

Due to the complexity of the problem of strong electronic correlations, in the present work we solve the single-band Hubbard Hamiltonian [15]. We use the Dynamical Mean-Field Theory (DMFT) [16, 17] and the continuous-time Quantum Monte Carlo solver in hybridization expansion (CT-HYB) [18]. The system Hamiltonian reads:

$$\hat{H} = \sum_{i,\sigma} (\sigma h - \mu)\hat{n}_{i\sigma} + \sum_{ij,\sigma} t_{ij}\hat{c}^{\dagger}_{i\sigma}\hat{c}_{j\sigma} + U\sum_{i} \hat{n}_{i\uparrow}\hat{n}_{i\downarrow}. \tag{1}$$

Here $\hat{c}^{\dagger}_{i\sigma}$ and $\hat{c}_{i\sigma}$ are the fermionic creation and annihilation operators at site i with spin σ. We denote the number operator at site i with $\hat{n}_{i\sigma} = \hat{c}^{\dagger}_{i\sigma}\hat{c}_{i\sigma}$. Furthermore, the parameter μ is the chemical potential, t_{ij} are the hopping matrix elements, and U is the Hubbard interaction. The hopping matrix is Hermitian $t_{ij} = t^{*}_{ji}$. We use a static Zeeman-like splitting h to generate half-metallicity in a one-band model. We use the density of states of a Bethe lattice with half-bandwidth fixed to $D = 1\,\mathrm{eV}$. Throughout the article, we fix the parameters to $\mu = -0.5\,\mathrm{eV}$ ($\mu' = -1.5\,\mathrm{eV}$ with respect to half filling), $h = 0.5\,\mathrm{eV}$ and $U = 2.0\,\mathrm{eV}$. While there exists a solution in one-dimensional systems [19], in higher dimensions we cannot solve this problem in general. The dynamical mean-field theory (DMFT) [4, 5], however, provides a non-perturbative approach, which can be applied for any range of parameters and is exact in the limit of infinite coordination number. It is furthermore exact for both solvable limits, the non-interacting limit $U = 0$ and the atomic limit $t_{ij} = 0$. The effective action within DMFT reads:

$$S_{eff} = -\int_0^{\beta} \mathrm{d}\tau \int_0^{\beta} \mathrm{d}\tau' \sum_{\sigma} c^{+}_{\sigma}(\tau)\mathscr{G}^{-1}_{0\,\sigma}(\tau - \tau')c_{\sigma}(\tau') + \int_0^{\beta} \mathrm{d}\tau U n_{\uparrow}(\tau)n_{\downarrow}(\tau) \tag{2}$$

where c^{+} and c are Grassmann fields. The bath Green's function writes for fermionic Matsubara frequencies

$$\mathscr{G}^{-1}_{0\,\sigma}(i\omega_n) = i\omega_n + \mu - \sigma h - \Delta(i\omega_n). \qquad i\omega_n = (2n+1)\pi T, n \in \mathbb{Z}, \tag{3}$$

where $\Delta(i\omega_n)$ denotes the hybridization function. The bath Green's function $\mathscr{G}_0$ is obtained from the lattice Green's function G_{lat}

$$\mathscr{G}^{-1}_{0}(i\omega_n) = 1/G_{\mathrm{lat}}(i\omega_n) + \Sigma(i\omega_n). \tag{4}$$

It is determined by the self-consistency condition

$$G_{\mathrm{lat}}(i\omega_n) \equiv G_{\mathrm{imp}}(i\omega_n), \tag{5}$$

where $G_{\mathrm{imp}\,\sigma}(\tau) = \langle c_{\sigma}(\tau)c^{+}_{\sigma}\rangle_{S_{eff}}$ is the Green's function of the effects action.

3. Finite temperature behavior of minority spin NQP states in bulk

In the simple one-band model HMFs are strong ferromagnets where the spin splitting exceeds the Fermi level, so that one spin subband is empty in the Hartree-Fock (Stoner)

picture. Difficulties in solving the Hubbard model for such a saturated ferromagnet are well known [7]. The electronic correlation effects in HMFs are connected with the occurrence of incoherent nonquasiparticle (NQP) states [2]. Note the clear distinction between the minority and majority half-metallic cases. The minority (majority) half-metal corresponds to almost empty (full) occupation; the NQP states are visible for the spin-down $\sigma =\downarrow$ (spin-up $\sigma =\uparrow$) electrons. As these states are situated just above (below) the Fermi level, they are expected to contribute to several physical properties such as: polarization, specific heat and transport.

Recent developments in the quantum Monte Carlo (QMC) technique [18] makes possible to significantly reduce the temperatures within the QMC calculations. Figure 1 shows our results

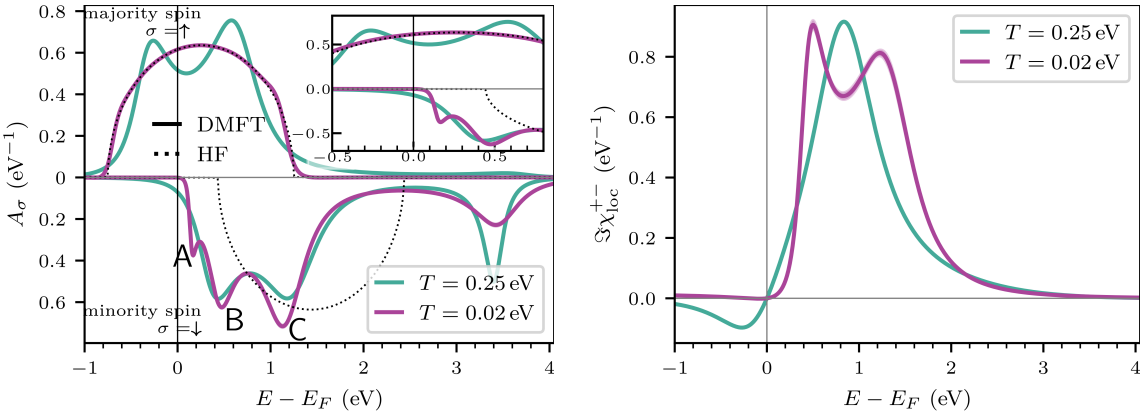

Figure 1. *Left*: Spin resolved spectral function $A_\sigma(E)$ for the half-metal. The purple (green) solid line represents DMFT results at low (high) temperatures $T = 0.02\,\mathrm{eV}$ ($T = 0.25\,\mathrm{eV}$). The high temperature result is in agreement with the previous calculations [10]. Black-dashed lines corresponds to the Hartree-Fock approximation.
Right: Real and imaginary part of the local spin-flip susceptibility corresponding to the spectra on the left side. We see that the peaks in the imaginary part of χ^{+-}_{loc} for $T = 0.02\,\mathrm{eV}$ agree reasonably well with the peaks B and C of the spectral function $A_{\sigma=\downarrow}$.

of the DMFT calculations. In the left graph, the green solid line shows the spectral function for high temperature ($T = 0.25\,\mathrm{eV}$), the purple solid line for low temperature ($T = 0.02\,\mathrm{eV}$). We use Padé approximants to analytically continue the lattice Green's function from Matsubara frequencies to the real axis. The black dotted line shows the simple Hartree-Fock solution as a comparison. The spectrum for high temperature agrees with the previous results [10], which were obtained using the simplified QMC scheme within the so-called exact enumeration technique [4]. For low temperatures the up-spin approaches the non-interacting results. The down-spin is almost depleted, thus the up-electron feels hardly any interaction; the absolute value of the self-energy is of the order of 10^{-5} to $10^{-4}\,\mathrm{eV}$.

At high temperature ($T = 0.25\,\mathrm{eV}$), the minority spin spectral function $A_\downarrow$ shows two peaks: B located at about $E - E_F \approx 0.5\,\mathrm{eV}$ and C located at about $E - E_F \approx 1.2\,\mathrm{eV}$. The peak B appearing in the spin-down gap was attributed [10] to the NQP state. This many-body feature describes a spin-polaron process [8]: the spin-down electron excitations forbidden in the one-electron description of HMF are possible due to the superposition of spin-up electron excitations and virtual magnons. In model calculations their existence has been proven by perturbation-theory arguments [7] for a broad-band case and in the opposite infinite-U limit [2,8]. In addition to the NQP states, a many-body satellite appears at $E-E_F \approx 3.5\,\mathrm{eV}$ in both spin channels. At low temperature ($T = 0.02\,\mathrm{eV}$), an additional peak A at

low frequency $E - E_F \approx 0.2\,\mathrm{eV}$ emerges in comparison to the high temperature results. A further reduction in temperature would lead to sharpening of the peak A. The peak A in the spectral function of the minority spin $\sigma = \downarrow$ corresponds to the position of the NQP state at low temperature, while the peaks B and C correspond to band edge effects enhanced by correlations. The left-hand side of Fig. 1 shows that the peak B corresponds to the spin down band edge, the peak C to the band edge in the spin-up channel. At high temperatures ($T = 0.25\,\mathrm{eV}$) the first two peaks A and B of the spectral function $A_\downarrow$ merge into a single peak, while the peak C present at low temperature is broadened and its weight is transferred into the high energy satellite at about 3.5 eV. To conclude the change of the spectral function $A_\downarrow$ with temperature, we note that the NQP peak A and the band edge peak B at low temperature $T = 0.02\,\mathrm{eV}$ merge to the single peak B at high temperature $T = 0.25\,\mathrm{eV}$.

As the origin of the NQP is a spin-polaron process, thus we also investigate the *local* spin-flip susceptibility of the impurity

$$\chi^{+-} = \left\langle S^+ S^- \right\rangle_{S_{eff}} = \left\langle c_\uparrow^+(\tau) c_\downarrow(\tau) c_\downarrow^+(\tau') c_\uparrow(\tau') \right\rangle_{S_{eff}} . \tag{6}$$

The brackets $\langle\cdot\rangle_{S_{eff}}$ denote the average in the effective impurity model. The right side of Fig. 1 shows the spin-flip susceptibility which was sampled using [20]. We compare the peak positions of the spectral function $A_\downarrow(E)$ with corresponding features of the imaginary part of the spin-flip susceptibility $\mathrm{Im}\,\chi^{+-}$. The low temperature spin-flip susceptibility shows a two peak structure, while at high temperatures a single peak is obtained. Currently its origin remains unexplained. The previous calculation [10] of the high temperature susceptibility used the bubble contribution only and obtained a two peak structure for the susceptibility $(\chi^{+-} + \chi^{-+})/2$. Here we see that the direct sampling of the two particle Green's function Eq. (6) at high temperature $T = 0.25\,\mathrm{eV}$ leads to a narrower peak and the disappearance of the two peak structure of the low temperatures.

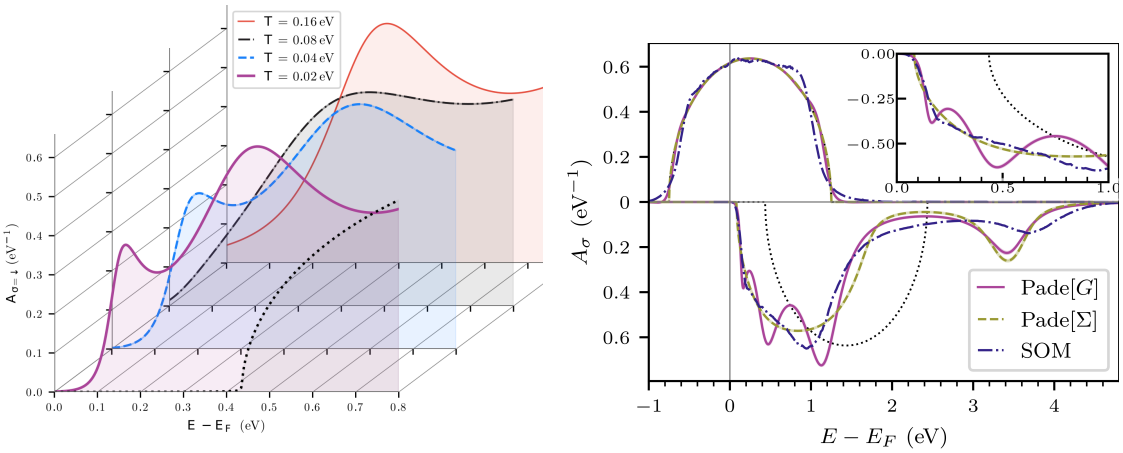

Figure 2. *Left*: Evolution of NQP in the minority spin spectral function $A_{\sigma=\downarrow}$ with temperature. This first line in the front corresponds to the low temperature result of Fig. 1, the other lines show logarithmetically increasing temperatures. *Right*: Comparison of different methods of calculating the analytic continuation for the spectral function for low temperature $T = 0.02\,\mathrm{eV}$. The purple line is the analytic continuation of the Green's function using Padé approximants shown in Fig. 1. The green line is obtained by continuation of the self-energy using Padé and applying the lattice Hilbert transform to the result. The blue line is produced by SOM [21]; 500 elementary, 5000 local and 1024 global updates were used. The dashed line gives the result of the Hartree-Fock approximation as a reference.

In Fig. 2 we study the systematic emergence of the additional low frequency peak for the minority spin $\sigma = \downarrow$. By reducing the temperature the peak emerges between $T = 0.08\,\mathrm{eV}$ and $T = 0.04\,\mathrm{eV}$. From the results presented above, we conclude that at these temperatures the spin-polaron mechanism forming the NQP states sets in.

4. Discussion and Conclusion

Difficulties in identifying features of the spectral function and susceptibilities may also be related to the analytical continuations used. We have used different ways to analytically continue the data as discussed in the following. On the left-hand side of Fig. 2, we see that the emergence of the NQP peak coincides with a significant reduction of the tail at the Fermi level. We may interpret this as a systematic error of the Padé approximants. Rational polynomials are not able to fit sharp edges or kinks, which can lead to wiggles, especially away from the Fermi level. The right graph of Fig. 2 compares the Padé approximation with the stochastic optimization method (SOM) [21]. For the spectral function of the majority spin $\sigma = \uparrow$, Padé produces good results; the result should approach the non-interacting spectral function. For the minority spin $\sigma = \downarrow$, the different methods disagree. If we use a Padé approximant for the self-energy and plug the continued self-energy into the lattice Hilbert transform, the resulting spectra shows no peaks at all. The conceptual advantage of using Padé in this fashion, is that we use the exact Hilbert transform and thus retain its branch cut; the Padé approximant of the Green's function replaces this branch cut by a finite number of poles. The disadvantage is that the self-energy contains more noise. At larger energies the unbiased results of SOM agree with neither of the Padé continuations. However, at the position of the NQP, the analytical continuation using SOM produces a shoulder.

To conclude, we studied the appearance of correlation induced features in the spectral function of the Hubbard model in the ferromagnetic fully polarized ground state. An external static magnetic field in form of a Zeeman term was used to produce the mean-field half-metallic ground state. The CT-HYB solver of the DMFT was used to obtain the spectral function and the spin-flip susceptibilities. Difficulties in identifying characteristics that are connected with the appearance of the NQP states are discussed, in particular the current comparison of different analytical continuations does not allow to clearly identify NQP features (peak vs. shoulder). A DMFT solver for real frequencies would reveal the specific features in discussion.

Acknowledgment

The authors acknowledge discussions with A. I. Lichtenstein. A. Weh acknowledges the hospitality of TU Wien and the discussions with K. Held, J. Kunes and M. Wallerberger. We acknowledges the financial support offered by the Augsburg Center for Innovative Technologies, and by the Deutsche Forschungsgemeinschaft (DFG, German Research Foundation), Project No. 107745057-TRR 80/G7.

References

[1] I. Zutic, J. Fabian, and S. Das Sarma, Rev. Mod. Phys. **76**, 323 (2004)

[2] M. I. Katsnelson, V. Y. Irkhin, L. Chioncel, A. I. Lichtenstein, and R. A. de Groot, Rev. Mod. Phys. **80**, 315 (2008)

[3] R. A. de Groot, F. M. Mueller, P. G. van Engen, and K. H. J. Buschow, Phys. Rev. Lett. **50**, 2024 (1983)

[4] A. Georges, G. Kotliar, W. Krauth, and M. J. Rozenberg, Rev. Mod. Phys. **68**, 13 (1996).

[5] D. Vollhardt, ArXiv:1910.12650 [Cond-Mat] (2019).

[6] T. Moriya, Spin Fluctuations in Itinerant Electron Magnetism, Springer Series in Solid-State Sciences, Springer Berlin Heidelberg, (2012)
[7] D. M. Edwards and J. A. Hertz, Journal of Physics F: Metal Physics **3**, 2191 (1973)
[8] V. Y. Irkhin and M. Katsnelson, Fizika Tverdogo Tela **25**, 3383 (1983)
[9] V. Y. Irkhin and M. I. Katsnelson, Phys. Usp. **37**, 659 (1994).
[10] L. Chioncel, M. I. Katsnelson, R. A. de Groot, and A. I. Lichtenstein, Phys. Rev. B **68**, 144425 (2003).
[11] L. Chioncel, E. Arrigoni, M. I. Katsnelson, and A. I. Lichtenstein, Phys. Rev. Lett. **96**, 137203 (2006).
[12] L. Chioncel, M. I. Katsnelson, G. A. de Wijs, R. A. de Groot, and A. I. Lichtenstein, Phys. Rev. B **71**, 085111 (2005).
[13] L. Chioncel, P. Mavropoulos, M. Lezaic, S. Bluegel, E. Arrigoni, M. I. Katsnelson, and A. I. Lichtenstein, Phys. Rev. Lett. **96**, 197203 (2006).
[14] L. Chioncel, H. Allmaier, E. Arrigoni, A. Yamasaki, M. Daghofer, M. I. Katsnelson, and A. I. Lichtenstein, Phys. Rev. B **75**, 140406 (2007).
[15] J. Hubbard, Proc. R. Soc. Lond. A **276**, 238 (1963).
[16] W. Metzner and D. Vollhardt, Phys. Rev. Lett. **62**, 324 (1989).
[17] G. Kotliar and D. Vollhardt, Physics Today **57**, 53 (2004).
[18] E. Gull, A. J. Millis, A. I. Lichtenstein, A. N. Rubtsov, M. Troyer, and P. Werner, Rev. Mod. Phys. **83**, 349 (2011)
[19] F. H. L. Essler, H. Frahm, F. Göhmann, A. Klümper, and V. Korepin, in Exactly Solvable Models of Strongly Correlated Electrons, Advanced Series in Mathematical Physics, World Scientific, vol. **18** (2010).
[20] M. Wallerberger, A. Hausoel, P. Gunacker, A. Kowalski, N. Paragh, F. Goth, K. Held, and G. Sangiovanni, Comput. Phys. Commun. **235**, 388 (2019)
[21] J. Nordström, J. Schött, I. L. Locht, and I. Di Marco, SoftwareX **5**, 178 (2016)